Carbon-Nanotube-Reinforced Zr-Based Bulk Metallic Glass Composites and Their Properties**

By *Zan Bian*, *Ru Ju Wang*, *Wei Hua Wang*,* *Tao Zhang*, and *Akihisa Inoue*

In this paper, we systematically report the preparation of carbon-nanotube (CNT)-reinforced Zr-based bulk metallic glass (BMG) composites. The physical and mechanical properties of the composites were investigated. Compressive testing shows that the composites still display high fracture strength. Investigation also shows that the composites have strong ultrasonic attenuation characteristics and excellent wave absorption ability. The strong wave absorption implies that CNT-reinforced Zr-based BMG composites, besides their excellent mechanical properties, may also have significant potential for applications in shielding acoustic sound or environmental noise.

1. Introduction

Since the first bulk metallic glass (BMG) was synthesized in 1989,[1] striking progress has been made in the preparation of BMGs. A great number of multicomponent metallic glass alloys with strong glass-forming ability (GFA) and high thermal stability have been found, such as, Zr, Fe, Pd, Nd, Pr, Mg, Ln, Cu, Ni, and other metallic glass alloy systems.[2–5] Because of their attractive properties, such as high yield strength, high elastic energy, high impact fracture energy, high hardness, good wear resistance, excellent corrosion resistance, and good castability as well as good soft and hard magnetism,[2–12] great attention has been paid to the formation mechanism, physical and mechanical properties, and potential engineering applications of these BMGs. Among them, Zr-based BMGs have been widely investigated because of their large GFA and high fracture strength, and they have already been introduced for commercial use in sporting goods materials, micromachines for fabricating various nanodevices, surgical instruments, very thin cases for electronic devices such as cell phones and computers, and other applications.

Recently, there has been considerable scientific and industrial interest in a variety of BMG composites as a way to further improve mechanical properties compared to monolithic BMGs. BMGs themselves are also interesting matrix materials for composites because of their low melting points of around 1000 K and their high resistance to heterogeneous nucleation of crystals. It has been found that BMG composites reinforced with metals or metal fibers[11,12] or ceramic particles[11,13–15] can significantly improve the fracture strength and plasticity of Zr-based BMGs. Conner et al.[11] prepared $Zr_{57}Nb_5Al_{10}Cu_{15.4}Ni_{12.6}$ BMG composites reinforced by metals or metal fibers or ceramic particles, such as W, WC, Ta, and SiC. Their results show that the compressive strain to failure increases by more than 300 % compared with the unreinforced BMG, and the fracture energy of the tensile samples increases by more than 50 %. The increase in toughness comes from the particles restricting shear band propagation, promoting the generation of multiple shear bands and additional fracture surface area. Pekarskaya et al.[16] and Hays et al.[17] also investigated the effect of ductile dendritic precipitates formed in situ and dispersed homogeneously in the BMG matrix on the mechanical properties, the plasticity, and the shear flow deformation of BMGs. Primary dendrite growth and solute partitioning in the molten state yields a microstructure consisting of a ductile crystalline Ti-Zr-Nb phase, with body-centered-cubic (bcc) structure, in a Zr-based BMG matrix. The dendritic microstructure of the Ti-Zr-Nb phase acts to seed the initiation of organized shear band patterns, confines the propagation of individual shear bands to domains having a spatial scale of the order of the primary dendrite axes length, may play a key role in initiating the formation of multiple shear bands, and leads to over 8 % of total strain (elastic and plastic) of the composites. More recently, Kim et al.[18] also reported that carbon-fiber-reinforced BMG composites can be prepared successfully by infiltrating liquid Zr-Ti-Cu-Ni-Be into carbon fiber bundles. The glassy state of the matrix was retained after processing. This suggested to us that carbon nanotubes (CNTs), as the "ultimate" carbon fiber and one of the stiffest structures ever made,[19,20] might be introduced into BMG matrix as a promising reinforcement. It is well-known that CNTs possess not only extremely high elastic moduli but also good plasticity.[19,20] The excellent mechanical properties and the chemical stability originate from their seamless cylindrical graphitic structure. BMG composites reinforced with CNTs might have unique properties such as high strength, light weight, stiffness, and so on. Furthermore, CNTs, which have attracted considerable interest

[*] Prof. W. H. Wang, Dr. Z. Bian, Prof. R. J. Wang
Institute of Physics, Chinese Academy of Sciences
Beijing 100080 (P.R. China)
E-mail: whw@aphy.iphy.ac.cn
Dr. Z. Bian, Dr. T. Zhang, Prof. A. Inoue
Institute for Materials Research, Tohoku University
Sendai 980-8577 (Japan)

[**] The authors are grateful for the financial support of the Natural Science Foundation of China (grant nos. 50201019, 50031010, and 59925101), Chinesisch-Deutsches Zentrum für Wissenschaftsförderung (grant no. GZ032/7), and 21st century COE (Center of Excellences) program of the Institute for Materials Research of Tohoku University (Japan). Thanks go to Dr. C. L. Xu for providing the carbon nanotubes.

 DOI: 10.1002/adfm.200304422

in both academia and industry, themselves also have some special functional properties, suggesting that it is possible that BMG composites containing CNTs would have some special functional properties.

In this paper, we report our successful attempt to prepare CNT-reinforced Zr-based BMG composites. A $Zr_{52.5}Cu_{17.9}Ni_{14.6}Al_{10}Ti_5$ alloy is used as a matrix material, which is one of the best glass-forming alloys developed so far. Physical properties and mechanical properties of the composites were investigated. Compressive testing shows that the composites still display high fracture strength. Investigation also shows that the composites have strong ultrasonic attenuation characteristics and excellent wave absorption ability. The strong wave absorption ability implies that CNT-reinforced Zr-based BMG composites, besides their excellent mechanical properties, may also have significant potential applications in shielding acoustic sound or environmental noise.[21]

2. Results and Discussions

2.1. Preparation of BMG Composites with CNT Addition

Figure 1 shows typical X-ray diffraction (XRD) patterns of Zr-based BMG composites with different volume fractions of CNTs. For the BMG composite containing 1 vol.-% CNTs

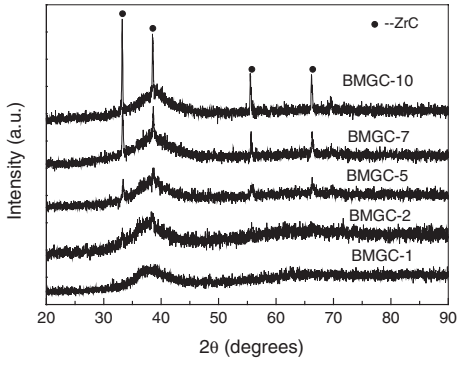

Figure 1. XRD patterns of Zr-based BMG composites containing different volume fractions of carbon nanotubes.

(BMGC-1), no crystallinity was detected within the sensitivity limit of XRD. For BMG composites containing 2.0, 3.0, 5.0, 7.0, and 10.0 vol.-% CNTs (BMGC-2, BMGC-3, BMGC-5, BMGC-7, BMGC-10), their XRD curves show a superimposition of a broad maximum from the amorphous phase and several sharp peaks characteristic of a crystalline phase, suggesting that a mixed structure of the amorphous and some crystalline phases is formed. The position and the intensity of the crystalline peaks match exactly with that of ZrC phase as shown in Figure 1. No other phases are detected within the sensitivity limit of XRD. This suggests that the some added CNTs have reacted partially with elemental Zr and formed crystalline ZrC. Zirconium has a much larger negative heat of mixing (109 kJ mol^{-1})[22] with C than that of other constituents (Al, Cu, or Ni), meaning that Zr and C have the largest driving force for the interfacial reaction. Thus, the C and Zr reaction is favored during the melting and casting processes, and leads to the formation of ZrC. Similar results were reported by others on introducing carbon fibers or elemental carbon into a BMG matrix.[15,18,23,24] As a comparison, Figure 2 shows XRD patterns of the pure as-cast CNTs, undoped BMG, and BMGC-3. No CNT peaks were observed in the XRD pattern of BMGC-3. This suggests that a small volume fraction of residual CNTs dispersed in the glass matrix is difficult to detect within the sensitivity limit of XRD. Other methods are needed to confirm the dispersion of CNTs in the glass matrix. This will be shown in a later section.

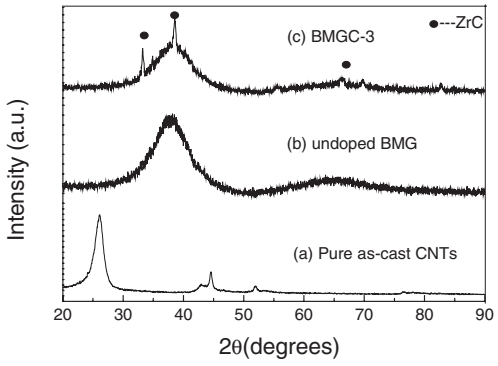

Figure 2. XRD patterns of the pure as-cast CNTs (a), undoped BMG (b), and a BMG-CNT composite (c).

Figure 3 shows differential scanning calorimetry (DSC) traces of the as-cast $Zr_{52.5}Cu_{17.9}Ni_{14.6}Al_{10}Ti_5$ BMG and the composites with different volume fractions of CNT additions (the heating rate is 20 K min^{-1}). DSC traces show that both the undoped BMG and the composite samples exhibit an endothermic feature, characteristic of the glass transition, followed by several characteristic exothermic heat events, indicating the successive stepwise transformation from the super-

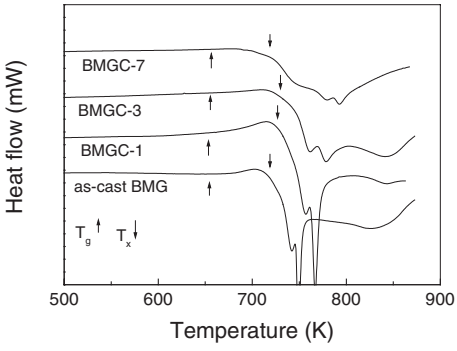

Figure 3. DSC traces of the as-cast $Zr_{52.5}Cu_{17.9}Ni_{14.6}Al_{10}Ti_5$ BMG and the composites containing different volume fractions of CNTs (the heating rate is 20 K min^{-1}).

cooled liquid state to crystalline phases (for the composites with more than 3.0 vol.-% CNT, the endothermic event is not so obvious compared with that of undoped BMG on the same heat flow scale, because glass friction in the composites decreases with more CNT addition. However, the endothermic

ADVANCED FUNCTIONAL MATERIALS

event does exist if the heat-flow scale is enlarged, because the ZrCuNiAlTi glass-forming alloy has a large glass-forming composition range, and the reaction between carbon and Zr does not significantly change the glass-transition behavior of the alloy[17,18,24]). The crystallization behavior is very different from that of the undoped BMG. For BMG composites with less than 3.0 vol.-% CNT additions, the glass-transition temperature, T_g, of the samples is not obviously different from that of the undoped BMG, but the onset temperatures, T_x, of all the crystallization peaks of the composite shift to higher temperature. A possible reason for this is that the matrix composition in the composite varies during the interfacial reaction between the added CNTs and the glass phase. In this process, some carbon atoms dissolve into the amorphous matrix of the composite and increase its packing density, leading to an increase of the thermal stability. The role of carbon atoms has also been reported by other researchers.[15,18,24] However, when the volume fraction of CNT addition is more than 7.0 vol.-%, one can observe that the T_x of the composite shifts to lower temperature. This result implies that more than 7.0 vol.-% CNT additions decreases the supercooled liquid region ΔT ($\Delta T = T_x - T_g$) of the glass matrix. However, as the Zr-based alloy has very strong glass-formation ability, a small decrease in ΔT does not affect the preparation of BMG composites, as shown in Figure 1. The larger volume fraction of CNTs leads to an increased probability of the interfacial reaction, and an increased volume fraction of crystalline ZrC. This results in a significant depletion of elemental Zr in the glass matrix. This is one important reason for the decrease in ΔT.[18]

To confirm that the CNTs have been incorporated in the BMG matrix, we carried out transmission electron microscopy (TEM) and high-resolution TEM (HRTEM). Figure 4a shows the typical morphology of as-prepared CNTs as revealed by TEM. The tubular shape is clearly observed. Some CNTs cluster closely together. Some CNTs are completely separate from each other. Figures 4b–4d show typical TEM images of the CNTs added to the BMG matrix. Figure 4c is an enlarged image of region B in Figure 4b. After CNTs have been added to the BMG matrix, whole CNTs and their tubular structure are clearly observed (Fig. 4b). Clusters of added CNTs are also observed, as shown in Figure 4d. Several CNTs cluster closely together, and remain so after the interfacial reaction. In Figures 4b,c, one can find a few V-shaped nicks caused by the interfacial reaction present on the edge of tubular CNTs (Fig. 4c). To further investigate the structural variation of CNTs after being distributed in the BMG matrix, HRTEM observation of CNTs themselves was also carried out (shown in Fig. 5). It is clearly seen that CNTs still keep their cylindrical graphitic structure, and the unique multi-walled structure still exists. This means that the CNTs dispersed in the glass matrix still basically keep their primary structure, implying that the added CNTs possibly keep their excellent mechanical and functional properties. In fact, whole CNTs have also been observed in fine powders of the composites, confirming the existence of CNTs in the composites (see Sect. 4.2.). The above results demonstrate that CNTs have been introduced into the BMG matrix and some of them still keep their unique multi-

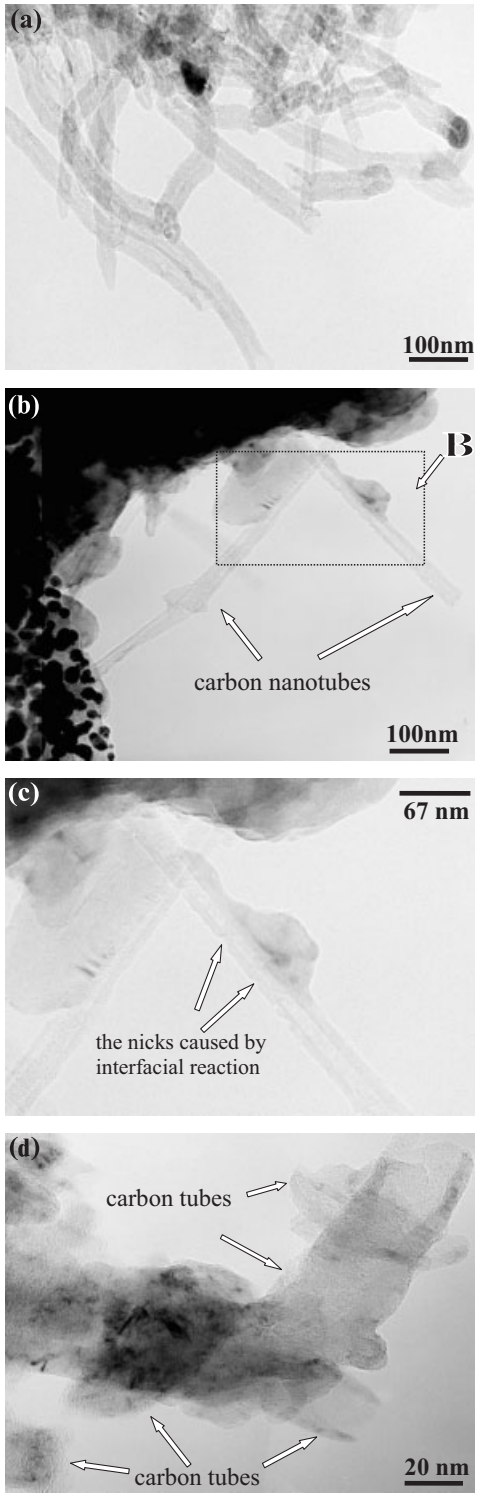

Figure 4. TEM morphology of CNTs distributed in a Zr-based BMG matrix. a) Typical HRTEM morphology of the as-prepared CNTs. b) Note that the tubular shape of the added CNTs is retained. c) Enlarged image of region B in (b). d) CNTs are also found in clusters.

walled structure. The reason for the distribution of CNTs in the glass matrix is the high thermal and chemical stability of the CNTs themselves,[19,20] and the low melting point (about

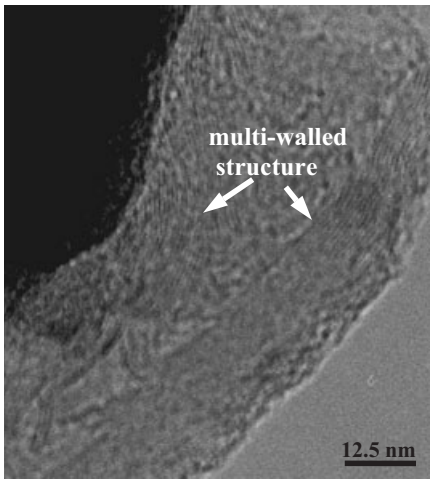

Figure 5. HRTEM morphology shows that the CNTs still keep their multi-walled structure after being distributed in the BMG matrix.

1100 K) and strong glass-forming ability of the $Zr_{52.5}Cu_{17.9}Ni_{14.6}Al_{10}Ti_5$ alloy.

2.2. Microstructure, Ultrasonic Properties, and Elastic Constants of BMG Composites with CNT Addition

Adding CNTs to the BMG matrix causes the formation of a mixed structure of residual CNTs and ZrC-phase dispersed randomly in the glass matrix. The mixed structure is also confirmed by TEM observation of the microstructure of the composites. Figure 6 shows a typical morphology as observed by TEM of CNTs dispersed in the BMG matrix, obtained from BMGC-3. Figures 6b,d are enlarged images of regions A and B, respectively, in the image of Figure 6a. The selected-area diffraction pattern (SADP) (Fig. 6c) in the matrix of the composites shows that the glass state of the matrix is still retained. From Figures 6a–6f, one can see that the CNTs have reacted partially with the glass matrix, but most of them are still kept in the BMG matrix. Figure 6e is the SADP of the interfacial region (region C in Fig. 6d) between the added CNTs and the glass matrix, which implies that the interfacial region is not completely amorphous. From Figure 6d, ZrC phase is also found (shown in region D of Fig. 6d), and its SADP is shown in Figure 6f. CNTs and ZrC-phase dispersed in the glass matrix have an obvious effect on the physical properties of BMGCs. Table 1 summarizes the density (ρ), longitudinal and transverse acoustic velocities (v_l and v_t), Young's modulus (E), shear modulus (G), bulk modulus (K), and hardness (H_V) of BMGCs containing different volume fractions of CNTs added. All the parameters increase with increasing CNT addition except the density, implying that the addition of CNTs to the BMG matrix plays an effective strengthening role. The reduced densities of BMG composites result from the low density of CNTs themselves (1.8 g/cm^3). Relative changes ($\Delta Y/Y_0 = (Y - Y_0)/Y_0$, where Y_0 represents the parameters of the undoped BMG and Y the parameters of BMGCs) in ν_l and ν_t are shown in Figure 7. The relative changes in ν_l and ν_t increase with increasing CNT addition. There are two reasons for the increase: 1) the precipitation

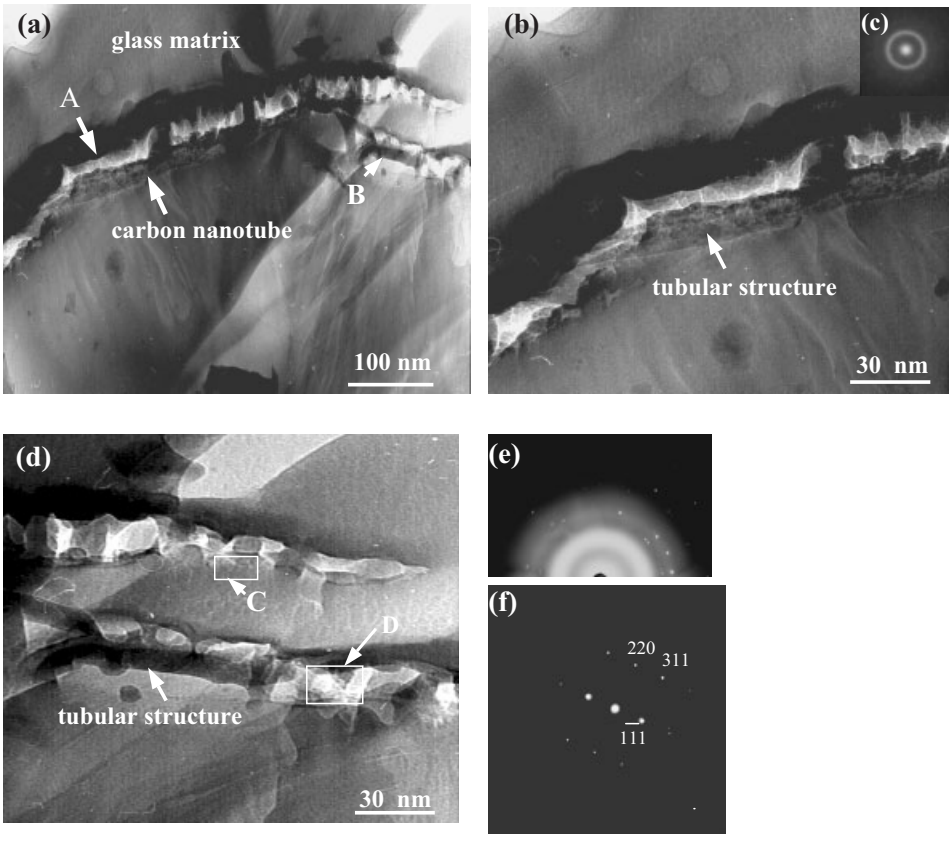

Figure 6. Typical TEM morphology of the microstructure of BMG composites containing CNT additions. a) The added CNTs disperse randomly in the glass matrix. b,d) Enlarged images of regions A and B in (a), respectively. c,e,f) Selected area diffraction patterns (SADPs) of the matrix in the composite, the interface between the glass matrix and the residual CNTs (region C), and ZrC phase (region D), respectively.

ADVANCED FUNCTIONAL MATERIALS

Table 1. The density ρ, longitudinal and transverse acoustic velocities (v_l and v_t), Young's modulus E, bulk modulus K, shear modulus G, and Vickers hardness (H_V) for the undoped BMG and the BMG composites containing different volume percentage CNT additions.

Alloy	ρ [g/cm^3]	v_l [km/s]	v_t [km/s]	E [GPa]	G [GPa]	K [GPa]	H_V
BMG	6.73	4.83	2.19	88.56	32.31	114.12	579
1.0 vol.-%	6.701	4.87	2.22	90.41	33.03	114.89	591
2.0 vol.-%	6.643	4.96	2.26	92.90	33.93	118.19	612
3.0 vol.-%	6.607	5.13	2.281	94.66	34.38	128.04	626
4.0 vol.-%	6.549	5.37	2.33	98.49	35.58	141.41	654
5.0 vol.-%	6.502	–	–	–	–	–	678
7.0 vol.-%	6.345	–	–	–	–	–	693
10.0 vol.-%	6.161	–	–	–	–	–	711

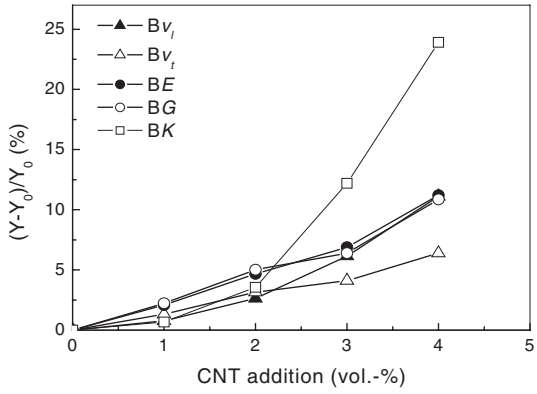

Figure 7. Relative changes $[(Y - Y_0)/Y_0]$ of the longitudinal and transverse acoustic velocities (v_l and v_t), and the elastic constants (E, K, G) of Zr-based BMG composites with increasing volume fraction of carbon nanotube addition. (Y_0 is the parameter of the BMG; Y is the parameter of the composite.)

of crystalline ZrC leads to the increase of acoustic velocity;[24,25] 2) carbon atoms dissolving into the amorphous matrix of the composite can increase its packing density and lead to an increase of acoustic velocity.[15,24–26] The relative changes in E, K, and G are also shown in Figure 7. The relative changes of BMGCs also increase with increasing volume fraction of CNT addition. The relative changes in E, K, and G are up to 11.21 %, 23.91 %, and 10.86 % for the composites containing 4.0 vol.-% CNT. A significant increase in E, K, and G suggests that CNTs in the BMG matrix play an effective role as a dispersed strengthener. This is also confirmed by the variation of H_V with increasing addition of CNTs. From Table 1 and Figure 8, one can seen that H_V increases greatly with increasing addition of CNTs. Chen et al.[23] have reported that the mixed structure of nanocrystalline phase and ZrC-phase dispersed randomly in the glass matrix is obtained by introducing carbon powder into the

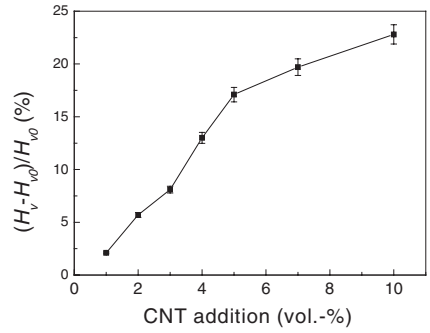

Figure 8. Relative changes $[(H_V - H_{V0})/H_{V0}]$ of the Vickers hardness of Zr-based BMG composites with increasing volume fraction of CNT additions. (H_{V0} is the Vickers hardness of the BMG; H_V is the Vickers hardness of the composite.)

BMG matrix. The nanocrystalline phase, which has a higher hardness than the glass matrix, improves significantly the mechanical properties of the composites. The microstructure of composites containing CNT addition is similar to that of composites with carbon powder addition after annealing,[21,24] which consists of the glass matrix, residual CNTs, and ZrC phase. It is well known that CNTs also have very high hardness and are one of the stiffest structures ever made.[19,20] CNTs dispersed in the BMG matrix still partially keep their tubular shape and unique multi-walled structure as shown in Figures 4 and 5, and thus the residual CNTs in the BMGCs can still keep their excellent mechanical properties. So, the dispersed strengthening of nanoscale CNTs and ZrC phase is the main reason for the increase in E, K, G, and H_V.

2.3. Ultrasonic Attenuation and Ultrasonic Wave Absorption Ability of BMG Composites Containing CNT Addition

The formation of the mixed structure of residual CNTs and ZrC phase dispersed randomly in the BMG matrix suggests that large numbers of nanoscale tubes are distributed randomly in the amorphous matrix. In this structure, there exist large amounts of new interface originating from the interfacial reaction between the added CNTs and the glass phase. This special structure can cause a strong acoustic wave attenuation and absorption (shown in Table 2). The values of longitudinal and transverse ultrasonic attenuation (α_l and α_t) increase significantly with increasing CNT addition. For BMGC-4, α_l is about 10 times and α_t nearly 7 times the corresponding values of the undoped BMG. The relative changes in α_l and α_t are shown in Figure 9. Even 1 vol.-% CNT addition causes very large relative changes in α_l and α_t (440 % and 255 %, respectively). The relative changes in α_l and α_t for BMGC-2, BMGC-3, and

Table 2. The longitudinal and transverse ultrasonic attenuation (α_l and α_t) for the undoped BMG and the BMGCs containing different volume fractions of CNTs.

	BMG	1.0 vol.-%	2.0 vol.-%	3.0 vol.-%	4.0 vol.-%	5.0 vol.-%	7.0 vol.-%	10.0 vol.-%
α_l [dB/cm]	0.5	2.7	3.3	3.7	5.0	–	–	–
α_t [dB/cm]	1.1	3.9	5.4	6.4	7.0	–	–	–

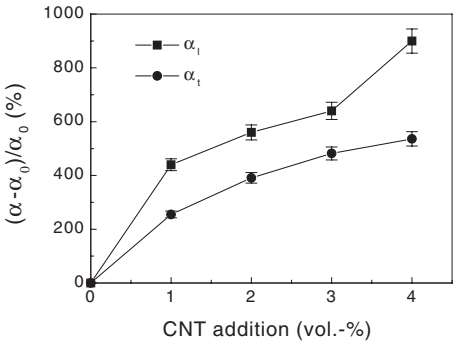

Figure 9. Relative changes [$\Delta\alpha/\alpha_0 = (\alpha - \alpha_0)/\alpha_0$] of the longitudinal and transverse ultrasonic attenuation (α_l and α_t) of Zr-based BMG composites with volume fraction of CNT addition. (α_0 is the attenuation coefficient of the undoped BMG; α is the attenuation coefficient of the composite.)

BMGC-4 are 560 %, 640 %, 900 % and 391 %, 482 %, 536 %, respectively. For BMGC-5, BMGC-7, and BMGC-10 samples, the values of acoustic velocities could not be detected because ultrasonic attenuation is too strong for a pulse echo to be observed on the screen under the applied experimental frequency. The above results imply that the addition of CNTs to a Zr-based BMG matrix causes strong ultrasonic attenuation and wave absorption. The strong absorption originates from the structural variation induced by adding CNTs to the BMG matrix.

It is well known that ultrasonic wave attenuation consists of wave absorption and scattering,[27] namely, the ultrasonic attenuation coefficient is expressed by $\alpha = \alpha_a + \alpha_s$ (where α_a is the absorption attenuation coefficient and α_s the scattering attenuation coefficient). For metallic glass alloys, the anharmonicity in a homogeneous solid gives rise to wave absorption via the so-called Akhieser effect.[28] The loss originates because under stress the phonons of an anharmonic solid shift to a new non-equilibrium distribution. For multiphase solids, acoustic attenuation originates from multiple scattering at multiple scatterers dispersed randomly in an elastically isotropic matrix. After adding CNTs to a BMG matrix, as shown in Figures 4–6, the residual CNTs still keep their tubular and multi-walled structure. These CNTs dispersed randomly in the glassy matrix supply large numbers of nanoscale tubes embedded randomly in the glass matrix. The interfacial reaction between the glassy matrix and the added CNTs also leads to the formation of small amounts of new interfaces and ZrC phase. The mixed structure of nanoscale tubes, the complex interfaces, and crystalline ZrC can act as strong multiple scatterers. Morse[29] reported that the scattered wave spreads isotropically in all directions at low frequencies when the wavelength of an incident wave (λ) is much greater than the particle radius (D). The wavelength of an ultrasonic wave with a frequency of 10 MHz is much larger than the mean size of CNTs. When waves were transmitted across composites with the mixed structure, most of them were multiply scattered in all directions because of the random distribution of multiple scatterers. This is the main reason for the strong wave absorption ability of BMG composites. Testardi et al.[28] and Maris[30] have reported that acoustic attenuation in amorphous solids caused by anharmonicity increases proportional to the square of the incident frequency, namely, $\alpha_a \propto f^2$. However, for a solid containing the multiple scatterers, attenuation will obey a varied law of frequency depending on the diameters, volume fractions, and mass of the scatterers, and other complex factors. From Table 1 and Figure 9, ultrasonic attenuation increases significantly with an increasing volume fraction of CNTs. It means that the volume fraction of CNTs dispersed in the glass matrix also has a significant effect on ultrasonic attenuation. Challis[31] has reported that the scattering efficiency P ($P = E^{(s)}/E^{(0)}$, where $E^{(0)}$ and $E^{(s)}$ are the energy per unit time of the incident wave and the scattered wave, respectively) arising from mass defects is proportional to $(\Delta m)^2 f^5$, namely, $P \propto (\Delta m)^2 f^5$, where Δm is the variation in the mass due to the introduction of the defects and f is the frequency of the incident wave. As the used frequency is 10 MHz, one can conclude that $P \propto (\Delta m)^2$, namely, $P \propto (\Delta\rho)^2$ (where $\Delta\rho = \rho - \rho_0$ and ρ and ρ_0 are the density of the BMG and the composites, respectively). Figure 10 shows the dependence of $(\Delta\rho)^2$ (or P) on the volume fraction of CNT addition. It is seen that $(\Delta\rho)^2$ (or P) increases significantly with increasing addition of CNTs, implying that the scattering efficiency P increases significantly with increasing CNT content. When the fraction of CNT addition is more than 5.0 vol.-%, P increases very rapidly. This means that we were unable to obtain a pulse echo and attenuation coefficient for BMGC-5, BMGC-7, and BMGC-10 under the applied experimental conditions. When the addition of CNTs increases, the total volume of the scattering phases per unit volume also increases. This raises the probability that an impinging wave will be scattered, and results in the increase of P. On the other hand, the compositional variation of the glass matrix also contributes to the increase of attenuation. In the process of the interfacial reaction between the added carbon nanotubes and the glass matrix, the dissolution of carbon atoms into the glass matrix induces a denser random packed microstructure of the glassy matrix, and results in stronger interatomic interaction and larger anharmonicity. This also causes the increase in ultrasonic absorption.[32]

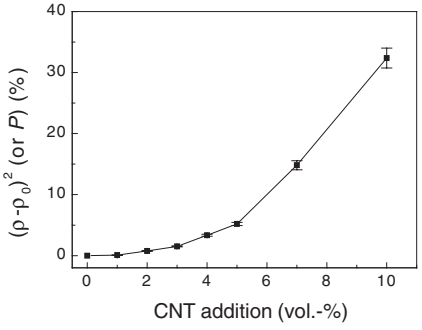

Figure 10. Dependence of $(\Delta\rho)^2$ (or the scattering efficiency P) on the volume fraction of carbon nanotubes added.

ADVANCED FUNCTIONAL MATERIALS

2.4. Mechanical Properties of BMG Composites Containing CNT Addition

Figure 11 shows compressive load–displacement curves of BMGCs containing different volume fractions of CNT addition. For the undoped BMG sample, a quite classical elastic–perfectly plastic appearance can be observed (Fig. 11a),

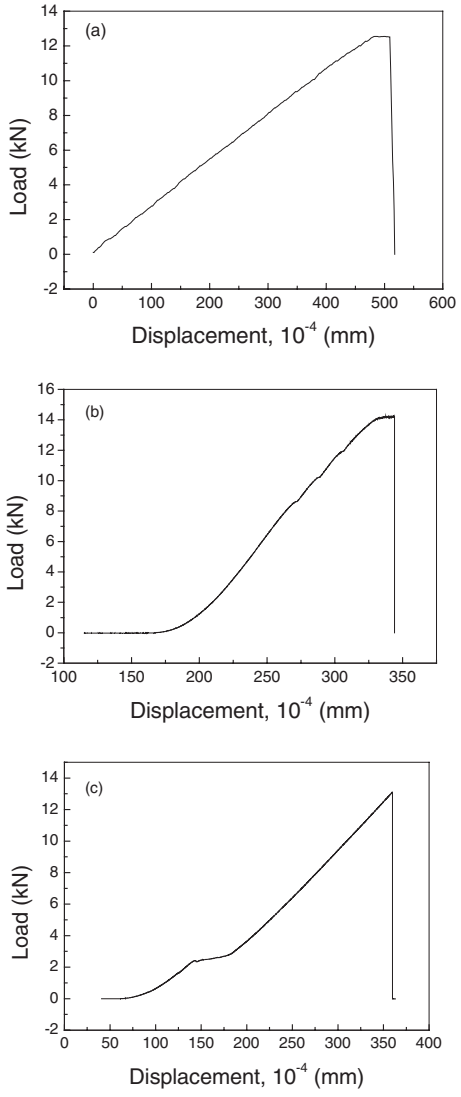

Figure 11. Compressive load–displacement curves of BMG composites containing different volume fractions of CNTs at a strain rate of 10^{-4} s^{-1}: a) the undoped BMG; b) BMG composite containing 3.0 vol.-%; c) BMG composite containing 7.0 vol.-%.

namely, predominantly elastic behavior followed by yielding and subsequent flow along shear bands up to fracture. The fracture strength, estimated according to $\delta = F_{max}/s$, where F_{max} is the maximum value of load and s is surface area of the top or bottom of the cylinders, is about 1770 MPa. For BMGCs containing 3.0 vol.-% CNT (Fig. 11b), the compressive load–displacement curve is very similar to that of the undoped BMG, namely, a quite classical elastic–plastic behavior followed by yielding and subsequent flow along shear bands up to fracture. The maximum fracture stress is about 1947 MPa. The value is much larger than the compressive fracture strength value of the undoped BMG. This result implies that the addition of CNT leads to obvious dispersion strengthening. But, with further increase in the addition of CNTs (more than 7.0 vol.-%), the load–displacement curves (Fig. 11c) show that the elastic behavior is followed by sudden fracture without shear flow deformation behavior, suggesting that BMG composites shift to brittle fracture. The fracture stress for BMGC-7 is 1873 MPa, and decreases gradually with increasing CNT addition. Figure 12 displays the variation tendency of maximum fracture stress of BMG composites with increasing CNT addition. It can be noticed that a strengthening tendency gradually changes to the embrittling process with increasing CNT addition. In summary, the fracture stress of BMG composites increases with increasing CNT addition when the volume fraction of CNT addition is less than 5.0 vol.-%. However, when CNT addition is more than 7.0 vol.-%, BMG composites display brittle fracture. In this case, the fracture stress decreases gradually with increasing CNT addition, as shown in Figure 12.

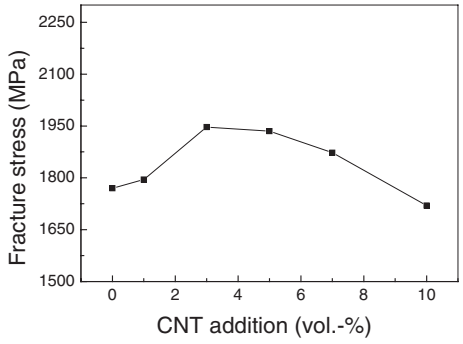

Figure 12. The dependence of fracture stress of BMG composites on the volume fraction of carbon nanotubes added.

From the above, the addition of CNTs forms a mixed structure of residual CNTs and ZrC phase randomly distributed in the BMG matrix, as shown in Figures 4,6. When a small volume fraction of CNT addition is distributed in the BMG matrix, it does not destroy the supercooled liquid regions of the BMG matrix, as shown in Figure 3. The fracture behavior of BMG composites containing a small volume fraction of CNT addition is still controlled by shear flow deformation behavior, which is confirmed by the load–displacement curve (shown in Fig. 11b). During compressive deformation, nanoscale CNTs will obstruct the shear flow deformation of the glass matrix, and play an effective role as dispersed strengtheners. This is the main reason for the increase of the compressive fracture strength. When a large number of CNTs are added to the BMG matrix (more than 7.0 vol.-%), CNT additions reduce the supercooled region of the present BMG matrix, as shown in Figure 3. Although we do not detect the precipitation of other intermetallic compounds, the increase in the volume fraction of ZrC precipitates still causes a significant depletion of Zr in the matrix. This changes the composition of the amorphous matrix, and affects the fracture strength of the

composites. On the other hand, the increase in CNT addition will lead to increasing volume fraction of residual CNTs dispersed in the amorphous matrix. From Figures 4–6, one can notice large numbers of V-shaped nicks, which form in the interfacial reaction between the added CNTs and the glass phase, on the residual CNTs. These nicks may act as nuclei for microcracks, and promote the nucleation and propagation of microcracks. When a small volume fraction of CNTs is added, the total number of these nicks on the residual CNTs is not enough to affect shear flow deformation behavior of the amorphous matrix.[10,33] In this case, the fracture behavior of BMG composites is still controlled by shear viscous flow, and the dispersion of residual CNTs plays an effective strengthening role. However, when the volume fraction of CNT addition is larger (more than 7.0 vol.-%), the total number of these nicks is enough to destroy shear flow deformation behavior of the amorphous matrix. In this case, the fracture behavior of BMG composites is not controlled by shear viscous flow. Large numbers of microcracks nucleate and propagate from the nicks on the residual CNTs. The propagation model of the microcracks controls the fracture behavior of BMG composites. This is the reason for the brittle fracture of BMG composites containing more than 7.0 vol.-% CNT additions.

3. Conclusions

In conclusion, CNT-reinforced BMG composites have been produced successfully. The BMG composites are lightweight and have improved mechanical and physical properties compared to the BMG itself. The following conclusions can be drawn.

Microstructure of BMG composites: BMG composites containing CNT addition have a mixed structure of residual CNTs and ZrC precipitate dispersed randomly in the amorphous matrix. The residual CNTs still keep their special tubular structure. The unique multi-walled structure of CNTs is also kept. However, some nicks originating from the interfacial reaction between the added CNTs and the glass phase are also observed.

Basic physical parameters of BMG composites: The density (ρ) of BMG composites decreases with an increasing volume fraction of CNT addition. The longitudinal and transverse acoustic velocities (v_l and v_t), elastic constant (Young's modulus E, shear modulus G, bulk modulus K), and hardness (H_V) of BMG composites increase with increasing CNT addition. The relative changes in v_l, v_t, E, K, and G are up to 11.11 %, 6.39 %, 11.21 %, 23.91 %, and 10.86 %, respectively, for the composites containing 4.0 vol.-% CNT addition. A significant increase in v_l, v_t, E, K, and G suggests that the addition of CNTs in the BMG matrix plays an effective strengthening role.

The strengthening and embrittling effect of CNT addition: A small volume fraction of CNT addition (less than 5.0 vol.-%) cannot destroy shear flow deformation behavior of the amorphous matrix. The fracture behavior of BMG composites is still controlled by viscous shear flow behavior. The random distribution of residual CNTs and ZrC phase in the amorphous matrix has the role of effective dispersed strengthening. For BMG composites containing more than 7.0 vol.-% CNT addition, the nucleation and propagation of microcracks originating from the nicks on the edge of residual CNTs will control the fracture behavior of the composites. In this case, BMG composites will shift to brittle fracture. The fracture stress of BMG composites decreases with increasing CNT addition.

The CNT-reinforced composites have strong ultrasonic attenuation characteristics and excellent wave absorption ability. Ultrasonic attenuation coefficients are very sensitive to the addition of CNTs, and increase dramatically with increasing volume fraction of CNT addition. The excellent ultrasonic absorption ability of the composites originates from the strong multiple scattering induced by the mixed structure of residual CNTs and crystalline ZrC phase dispersed randomly in the glass matrix, and the interfaces between the glassy phase and CNTs. Our work shows that the composites might have potential applications in the field of shielding acoustic sound or environmental noise.

At present, the most important problem that we should solve is how to control or decrease the interfacial reaction between Zr and carbon nanotubes. If we can significantly weaken the interfacial reaction, the possibility of formation of nicks in the interfacial reaction will be reduced significantly, implying that much larger volume fractions of CNTs can be distributed in the BMG matrix and further improve the mechanical properties of BMG composites. Surface-coated carbon nanotubes may possibly solve this problem. This line of investigation will be followed.

4. Experimental

4.1. Preparation of BMG Composites

Ingots with a nominal composition of $Zr_{52.5}Cu_{17.9}Ni_{14.6}Al_{10}Ti_5$ were prepared by arc melting a mixture of high purity Zr, Al, Ni, Cu, and Ti under a Ti-gettered purified Ar atmosphere. The prealloyed ingots were broken into small parts and ground mechanically into fine powder with a particle size of about 200 μm. The carbon nanotube powder with a density of 1.8 g cm^{-3} was cleaned in acetone and dehydrated at 473 K. The ingot powder was mixed homogeneously with different volume fractions of carbon nanotube powder, and dried immediately in a vacuum furnace for 5 h. The mixed powder was compressed into cylinders with 40 MPa in steel dies (diameter 8 mm) for 60 min. The cylinders were melted in a quartz tube rapidly by induction under a high pure Ar atmosphere, and then cast into a copper mold quickly by applying an argon gas pressure of 600 mbar to produce composite rods (diameter 5 mm).

4.2. Characterization

X-Ray Diffraction (XRD): XRD data of the composites containing different volume fractions of carbon nanotube addition were analyzed using a MAC M03 XHF diffractometer with Cu Kα radiation.

Microstructure: The specimens for transmission electron microscopy (TEM) were prepared from thin slices cut from the rod and thinned electrochemically by jet polishing at 250 K, using a solution of CH_3COOH and $HClO_4$ in the ratio of 10:1. Subsequently, the specimens were ion beam thinned in an ion mill. The specimens were ob-

ADVANCED FUNCTIONAL MATERIALS

served by using a JEOL 1210 transmission electron microscope at 80 kV.

TEM Observation of As-Prepared Carbon Nanotubes: The powder of carbon nanotubes was placed on a copper grid covered with a thin carbon film, and observed using high-resolution TEM (HRTEM) in a JEM-200cx.

HRTEM Observation of Carbon Nanotubes Added to the BMG Matrix: The composite sample was broken into small parts, mixed with CH_3CH_2OH, and then mechanically ground into very fine powder. The fine powder was placed on a copper grid covered with a thin carbon film, and also observed using HRTEM in a JEM-200cx operating at 200 kV.

The Vickers hardness (H_V) of the composites containing the different volume fractions of carbon nanotube addition was measured using a Polyvar Met microhardness tester with a 200 g load. The accuracy lies within 3 %.

4.3. Compressive Testing for Mechanical Properties

The composite rods (diameter 3 mm) were cut into cylinders with a length of 5.1–5.3 mm. The ends of the cylinders were carefully polished flat and parallel. The compressive testing at room temperature was carried out at a strain rate of 10^{-4} s^{-1} using an Instron-type testing machine. The accuracy lies within 5 %.

4.4. Ultrasonic Measurements

The composite rods were cut into cylinders of length 8 mm. The ends of the cylinders were carefully polished flat and parallel. The acoustic velocities of the specimens at room temperature were measured using a pulse-echo overlap technique [34,35]. The travel time of ultrasonic waves propagating through the specimen with a 10 MHz frequency was measured using a MATEC 6600 ultrasonic system with a measured sensitivity of 0.5 ns.

The density of the sample was measured by the Archimedean technique; the accuracy lies within 1 %. Elastic constants (i.e., Young's modulus E, shear modulus G, bulk modulus K) of the BMG and the composites were obtained from the acoustic velocities and the densities [34,35].

Ultrasonic attenuation was obtained by measuring the amplitude decay of successive echoes. The attenuation coefficient (α [dB cm^{-1}]) of a sample is calculated according to [27]

$$\alpha = \frac{20}{2nl}\log\left(\frac{A_i}{A_{i+n}}\right) \quad (1)$$

where A_i and A_{i+n} indicate the amplitudes of the ith and $(i+n)$th echoes, respectively; l is the length of the sample. The measuring sensitivity of attenuation was about 5 %.

Received: May 23, 2003
Final version: August 6, 2003

[1] A. Inoue, T. Zhang, T. Masumoto, *Mater. Trans., JIM* **1989**, *30*, 965.
[2] a) A. Inoue, *Bulk Amorphous Alloys: Preparation and Fundamental Characteristics*, Trans Tech, Zürich **1998**. b) A. Inoue, *Bulk Amorphous Alloys: Practical Characteristics and Applications*, Trans Tech, Zürich **1999**.
[3] W. L. Johnson, *MRS Bull.* **1999**, 24(Oct), 42.
[4] H. C. Yim, D. H. Xu, W. L. Johnson, *Appl. Phys. Lett.* **2003**, *82*, 1030.
[5] T. Zhang, A. Inoue, *Mater. Trans., JIM* **2002**, *43*, 708.
[6] W. L. Johnson, *Mater. Sci. Forum* **1996**, *225–227*, 35.
[7] A. L. Greer, *Science* **1995**, *267*, 1947.
[8] R. Doglione, S. Spriano, L. Battezzati, *Nanostruct. Mater.* **1997**, *8*, 447.
[9] A. Leohard, L. Q. Xing, M. Heilmaier, A. Gebert, J. Eckert, L. Schultz, *Nanostruct. Mater.* **1998**, *10*, 805.
[10] Z. Bian, G. He, G. Chen, *Scr. Mater.* **2000**, *43*, 1003.
[11] R. D. Conner, H. Choi-Yim, W. L. Johnson, *J. Mater. Res.* **1999**, *14*, 3292.
[12] R. B. Dandliker, R. D. Conner, W. L. Johnson, *J. Mater. Res.* **1998**, *13*, 2896.
[13] H. Choi-Yim, W. L. Johnson, *Appl. Phys. Lett.* **1997**, *71*, 3808.
[14] H. Kato, A. Inoue, *Mater. Trans., JIM* **1997**, *38*, 793.
[15] W. H. Wang, Q. Wei, *Appl. Phys. Lett.* **1997**, *71*, 58.
[16] E. Pekarskaya, C. P. Kim, W. L. Johnson, *J. Mater. Res.* **2001**, *16*, 2513.
[17] C. C. Hays, C. P. Kim, W. L. Johnson, *Phys. Rev. Lett.* **2000**, *84*, 2901.
[18] C. P. Kim, R. Bush, A. Masuhr, H. Choi-Yim, W. L. Johnson, *Appl. Phys. Lett.* **1997**, *79*, 1456.
[19] M. M. Trancy, T. W. Ebbesen, J. M. Gibson, *Nature* **1996**, *381*, 678.
[20] E. W. Wong, P. E. Sheehan, C. M. Gibson, *Science* **1997**, *277*, 1971.
[21] Z. Bian, R. J. Wang, M. X. Pan, D. Q. Zhao, W. H. Wang, *Adv. Mater.* **2003**, *15*, 616.
[22] F. R. De Boer, R. Boom, W. C. M. Mattens, A. R. Miedema, A. K. Niessen, *Cohesion in Metals*, North-Holland, Amsterdam **1998**.
[23] F. Chen, M. Takagi, T. Imura, Y. Kawamura, H. Kato, A. Inoue, *Mater. Trans., JIM* **2002**, *43*, 1.
[24] a) W. H. Wang, Z. Bian, P. Wen, Y. Zhang, M. X. Pan, *Intermetallics* **2002**, *10*, 1249. b) W. H. Wang, H. Y. Bai, *Mater. Lett.* **2000**, *44*, 59.
[25] W. H. Wang, R. J. Wang, *Appl. Phys. Lett.* **1999**, *74*, 1083.
[26] L. M. Wang, W. H. Wang, R. J. Wang, Z. L. Zhao, Y. S. Yao, D. Y. Dai, L. L. Sun, W. K. Wang, *Appl. Phys. Lett.* **2000**, *77*, 1147.
[27] *Physical Acoustics VII* (Eds: W. P. Mason, R. N. Thurston), Academic, New York **1982**.
[28] L. R. Testardi, J. T. Krause, H. S. Chen, *Phys. Rev. B* **1973**, *8*, 4464.
[29] P. M. Morse, *Vibration and Sound*, McGraw-Hill, New York **1948**.
[30] H. J. Maris, in *Phonon Scattering in Condensed Matter*, Proc. of the 3rd Int. Conf. on Phonon Scattering in Condensed Matter, Brown University, August 1979 (Ed: H. J. Maris), Plenum, New York **1980**, p. 69.
[31] L. J. Challis, in *Phonon Scattering in Solids*, Proc. of the 2nd Int. Conf. on Phonon Scattering in Solids, University of Nottingham, August 1976 (Ed: H. J. Maris), Plenum, New York **1976**, p. 55.
[32] W. H. Wang, R. J. Wang, F. Y. Li, M. X. Pan, Z. C. Qin, D. Q. Zhao, Y. X. Zhuang, Y. Zhang. *J. Appl. Phys.* **2000**, *88*, 3266.
[33] Z. Bian, G. L. Chen, G. He, X. D. Hui, *Mater. Sci. Eng. A* **2001**, *316*, 135.
[34] D. Schreiber, *Elastic Constants and Their Measurement*, McGraw-Hill, New York **1973**.
[35] W. H. Wang, H. Y. Bai, J. L. Luo, R. J. Wang, D. Jin. *Phys. Rev. B* **2000**, *62*, 25.

